Methane Mobility and Fate in Groundwater Determined from a Controlled Release Field Experiment

Authors: Aaron G. Cahill[1], Colby M. Steelman[1], Olenka Forde[2], Olukayode Kuloyo[3], S. Emil Ruff[3], Bernhard Mayer[3], K. Ulrich Mayer[2], Marc Strous[3], M. Cathryn Ryan[3], John A. Cherry[1], and Beth L. Parker[1]*

Affiliations:

[1] G360 Centre for Applied Groundwater Research, University of Guelph, Ontario, Canada

[2] Department of Earth, Ocean and Atmospheric Science, University of British Columbia, British Columbia, Canada

[3] Department of Geoscience, University of Calgary, Calgary, Alberta, Canada

*Corresponding author email: bparker@uoguelph.ca

Summary

Expansion of shale gas extraction has fueled global concern about fugitive methane impacts on groundwater and climate. Although methane leakage from wells is common, information regarding impacts to groundwater remains sparse, and is believed by many to be minor. We injected methane gas into a shallow, flat-lying sand aquifer for 72 days. While a significant fraction of methane vented to the atmosphere, an equal portion remained in the groundwater. Methane migration in the aquifer was governed by subtle grain-scale bedding that impeded buoyant free-phase gas flow, leading to episodic releases of free-phase gas, and fostering lateral gas migration farther than anticipated based on groundwater advection. Methane persisted in the groundwater zone despite active growth of methanotrophic bacteria, while much of the methane venting into the vadose zone was degraded. Our results show even small-volume releases of methane gas cause extensive free-phase and solute plumes emanating from leaks only detectable using well-established contaminant hydrogeology monitoring methods.

Main Article Text

Unconventional petroleum development[1] has generated controversy regarding the occurrence, magnitude, and effects of fugitive methane leakage[2, 3] from imperfectly sealed well bores[4, 5]. Identifying the frequency, origin and pathways of fugitive methane in the subsurface[6, 7] are paramount to understanding its impacts on our fresh groundwater resources. Numerous field techniques have been developed in an attempt to detect methane leakage[8, 9, 10], while scenario-based numerical modelling has been used to assess subsurface behaviours[11]. However, no field research has specifically or comprehensively addressed methane migration and fate in the subsurface at high spatiotemporal resolution. Consequently, evidence-based conceptual understandings of fugitive methane distribution in freshwater aquifers remain weak despite expert panel recommendations[12, 13] to examine potential environmental impacts of expected widespread development of unconventional petroleum resources.

Methane leakages from oil and gas wells due to imperfect well bore seals are common[14]; the seals are formed of cement and are geochemically unstable in the saline formations through which the wells are emplaced[15], resulting in eventual deterioration and leakage. However, the controversy arises because the typical measurements conducted at well heads only considers gas leaking up along the well casings to atmosphere[16], and neglects the potential for methane escaping the well casing into adjacent geological formations and migrating within the subsurface, potentially impacting potable groundwater resources. A series of papers that relied only on sampling existing domestic and farm water wells in active shale gas plays in Pennsylvania[8, 17] claim that methane attributable to shale gas wells occurred within a kilometre of the well; however, other studies claim this methane is explained by processes not related to shale gas development[18, 19, 20]. Much of this debate originates from inherent ambiguities in

measurements obtained from domestic water wells[19] that are merely receptors of contaminants, as opposed to properly engineered groundwater monitoring systems[19, 21], with sufficient resolution to identify sources and mitigation options.

This paper presents the results of a multi-disciplinary experiment that examined the movement, impacts, and fate of free-gas methane injected into a shallow freshwater aquifer comprised of nearly homogeneous, Pleistocene beach sand located at CFB Borden, Ontario, Canada (Fig. 1a). We considered surface gas efflux and ground-penetrating radar (GPR) monitoring to track subsurface free-gas movement, along with aqueous chemistry (including dissolved gases and C and H isotope ratios of methane) and microbial characterization to assess the nature and extent of groundwater quality impacts in the well-characterized Borden aquifer[22, 23] under natural conditions of geologic heterogeneity, groundwater flow, and hydrochemistry.

Methane (~51 m^3 at standard temperature and pressure) was injected using electronic mass flow control valves simultaneously into two 45^o angled drive-point wells over 72 days at two depths situated at 4.5 and 9 m below ground surface (Fig. 1b). Total injection rates were 0.17, 1.0, and 4.3 $m^3 \cdot day^{-1}$ (Extended Data Table 1) and represent the low to median range in surface casing vent flows observed in Alberta and British Columbia, Canada[14]. Monitoring was performed for 245 days after start of injection. The aquifer consists of 9 m of horizontal, interconnected lenses ranging from silt to coarse-grained sand with limited heterogeneity, underlain by a silty-clay aquitard. Locally, the water table is 1 m below ground surface (±0.5 m from spring to fall, respectively). Concentrations of dissolved methane are naturally low (0.02 to 0.2 $mg \cdot L^{-1}$) and baseline methane is biogenic with potential methane oxidation ($\delta^{13}C$-CH_4 ranges from -80 to -48‰).

Monitoring of methane efflux was done at surface and in the thin vadose zone to determine upward movement and venting to the atmosphere (Fig. 1b, c). To also capture horizontal methane migration along bedding in the direction of groundwater flow, depth-discrete monitoring points were placed in the aquifer at multiple depths downgradient of the injectors (Fig. 1b, c). The groundwater monitoring network was designed based on previous Borden aquifer[24] and CO_2 gas injection experiments[25]. The upper injector is located in the aerobic zone and the lower one in the anaerobic zone where there is slightly higher baseline dissolved methane and increased sulfate.

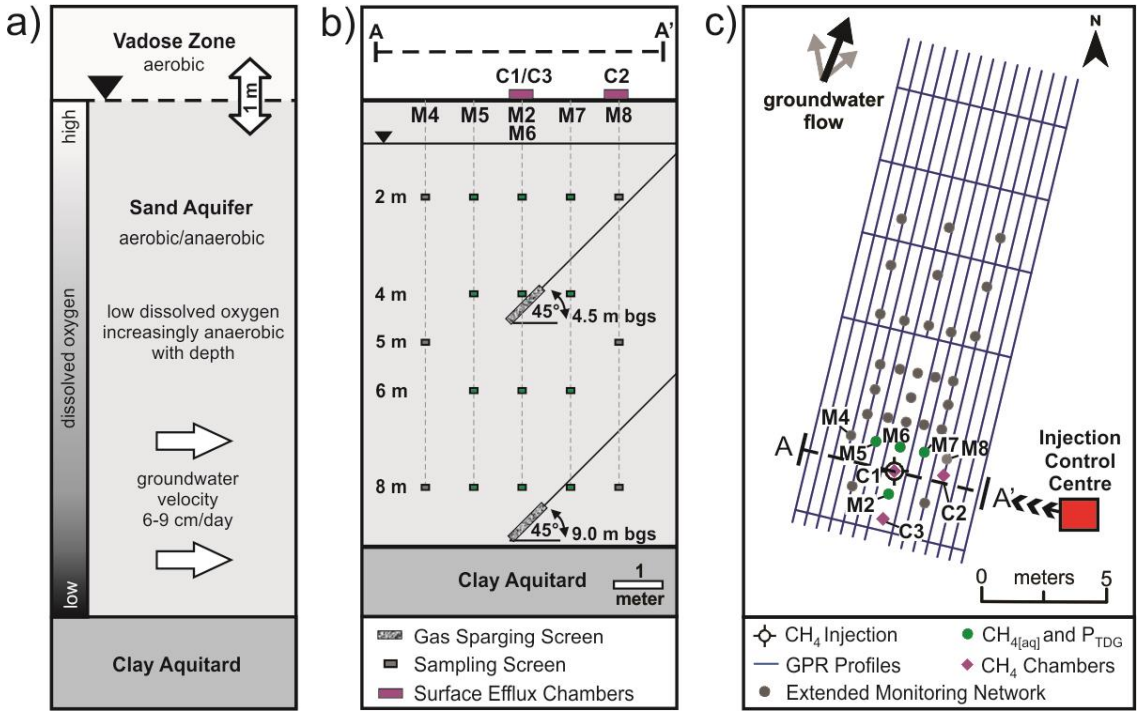

Fig. 1: (a) Hydrological setting of the Borden aquifer, consisting of a thin vadose zone and a relatively homogeneous sandy aquifer underlain by a clay aquitard. (b) Cross-section of groundwater monitoring network adjacent to injection points. (c) Plan-view of experimental design including extended groundwater monitoring network, surface efflux chambers, and geophysical profile lines. The injection control centre consisted of a mobile laboratory (for sample preparation/handling), methane canisters, and computer-controlled mass flow valves.

Our results show rapid and widespread migration of free-gas methane along bedding in the direction of groundwater flow accompanied by buoyancy-driven upward migration, rapidly causing a continuous, dispersed zone of dissolved methane and hydrochemistry changes (Figs. 2 and 3). Total dissolved gas pressure (P_{TDG}), which indicates the total amount of gas dissolved in water[26], evolved in an episodic manner (Fig. 2c) with pressure increases preceding build-up of $[CH_4]_{(aq)}$ (dissolved methane concentration). $[CH_4]_{(aq)}$ increased across all depths after a pause in gas injection (days 39 to 44), and after the injection stopped on day 72 (Fig. 2b), to concentrations that indicate explosion risk following ex-solvation into a confined space (>10 $mg \cdot L^{-1}$ as the accepted lower explosion limit)[27]. Upon resumption of methane injection on day 44, P_{TDG} increased or stabilized while $[CH_4]_{(aq)}$ decreased below the explosion risk limit (Fig. 2b, c). This temporary decrease in $[CH_4]_{(aq)}$ is potentially a result of displacement of CH_4-charged water by, or mixing with, un-impacted groundwater.

The injection of pressurized gas into a permeable geologic unit typically results in the formation of free-gas migration pathways or channels[28]. In our experiment, methane transfer from gaseous to aqueous phase appears limited during periods of free-gas migration or channelling[29]. Upon termination of methane injection, free-gas pressure decreases allow groundwater to re-saturate the pore space and increase surface area for transfer between gas and aqueous phases, resulting in the observed $[CH_4]_{(aq)}$ increases (Fig. 2b). While free-gas migration channelling is recognized as limiting subsurface gas retention and efficacy of air-sparging remediation strategies[30], its importance in the migration and fate of fugitive methane from energy resource development has not been rigorously explored.

The highest concentrations and spatial extent of $[CH_4]_{(aq)}$ occurred on day 113 (41 days following termination of gas injection), with concentrations >25 $mg \cdot L^{-1}$ (Extended Data Fig. 1). After 245

111 days, methane concentrations >10 mg·L^{-1} were observed at 2 and 6 m depths, demonstrating
112 persistence of injected methane (Extended Data Fig. 1).

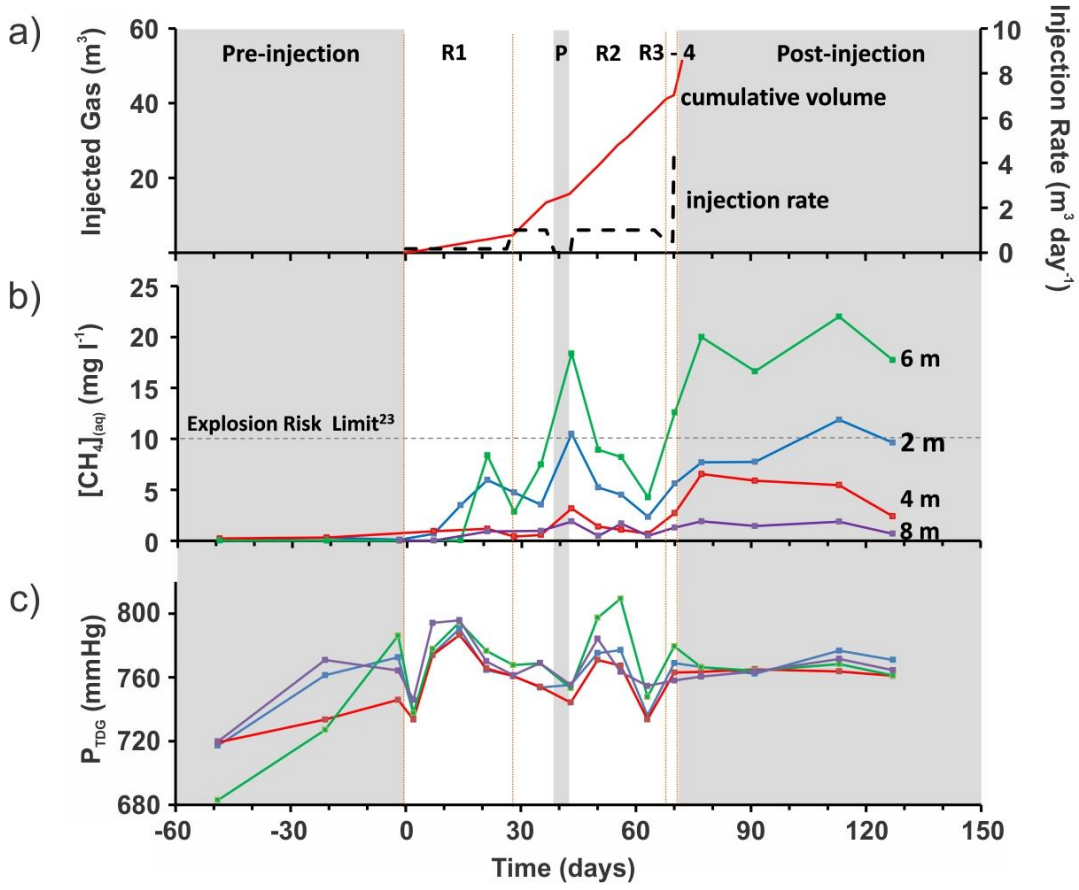

113

114 **Fig. 2:** a) Experimental timeline showing pre-injection monitoring period (-49 to 0 days),
115 injection rates employed (R1-R4) including cumulative volume of methane injected (0 to 72
116 days), and post-injection monitoring period (72 to 150 days); b) average $[CH_4]_{(aq)}$, and c) average
117 P_{TDG} with depth around the injection zone (i.e., for sample points M2, 5, 6, and 7; see Fig. 1c and
118 Methods). P_{TDG} and $[CH_4]_{(aq)}$ evolve in a staggered manner with pressure increases preceding
119 elevated $[CH_4]_{(aq)}$. Loss of gas injection pressure (pause or termination) induces depth discrete
120 increases in $[CH_4]_{(aq)}$.

121 Attenuation of $[CH_4]_{(aq)}$ and general water quality impacts were minimal at the time of last
122 sampling, showing slight increases in alkalinity (~4.3 to 5.3 meq·L^{-1}), decreases in pH (~7.3 to
123 7.0), and consistent increases in cation concentrations, including trace metals (e.g., Al, Ni, Sr),

directly around (1-2 m distance) the injection zone (Extended Data Table 2). The evolution of pH, alkalinity and aqueous Ca^{2+} (Extended Data Fig. 2) in the upper portion of the aquifer suggests microbial aerobic methane oxidation is generating CO_2, thereby leading to carbonic acid formation and acid-soluble (e.g., carbonate) mineral dissolution. Based on previous CO_2 experiments[31], carbonic acid-induced groundwater acidification may explain the increase in trace metals via dissolution and/or ion exchange processes. Although trace metals did not exceed drinking water limits over our monitoring period, these increasing trends may be of more significant concern given expected lifespans (decades) of shale gas wells[14]. Furthermore, the magnitude of water quality impacts will depend on the aquifer mineralogy. Given that the Borden sand is relatively inert (comprised primarily of quartz) [22], groundwater quality impacts in this experiment will be relatively low compared to deeper, more complex aquifers comprised of more reactive minerals.

Methane gas efflux was detected at ground surface within hours of starting the injection. An equally rapid cessation of surface effluxes was observed when injection was stopped. The surficial CH_4 emission area was dependent on the injection rate and resulted in a 'hotspot' offset 1 m from the injection point (Fig. 3a). Continuous long-term chambers (LTCs) captured a high degree of temporal variability in surficial gas effluxes (Fig. 3b). Effluxes were episodic throughout the experiment despite constant injection rates during each injection phase. Peak methane efflux rates at the three LTCs also varied spatially, even though the measurements were taken only 1 to 2 m apart (Extended Data Fig. 5). These spatiotemporal variations in efflux demonstrate the challenges associated with flux measurements and calculations, particularly those based on standard monitoring methods such as soil gas surveys, which have a much lower spatial resolution and are only conducted periodically.

A conservative estimate based on the integration of all methane efflux rates over the experimental time suggests that at least 30% of the injected methane was emitted into the atmosphere (Extended Data Table 3); an additional portion was likely emitted as CO_2 after CH_4 oxidation in the vadose zone. Substantial ^{13}C enrichment of gas-phase methane in the vadose zone resulting in $\delta^{13}C$ values as high as -20 to -15 ‰, provides strong evidence for microbially mediated methane oxidation.

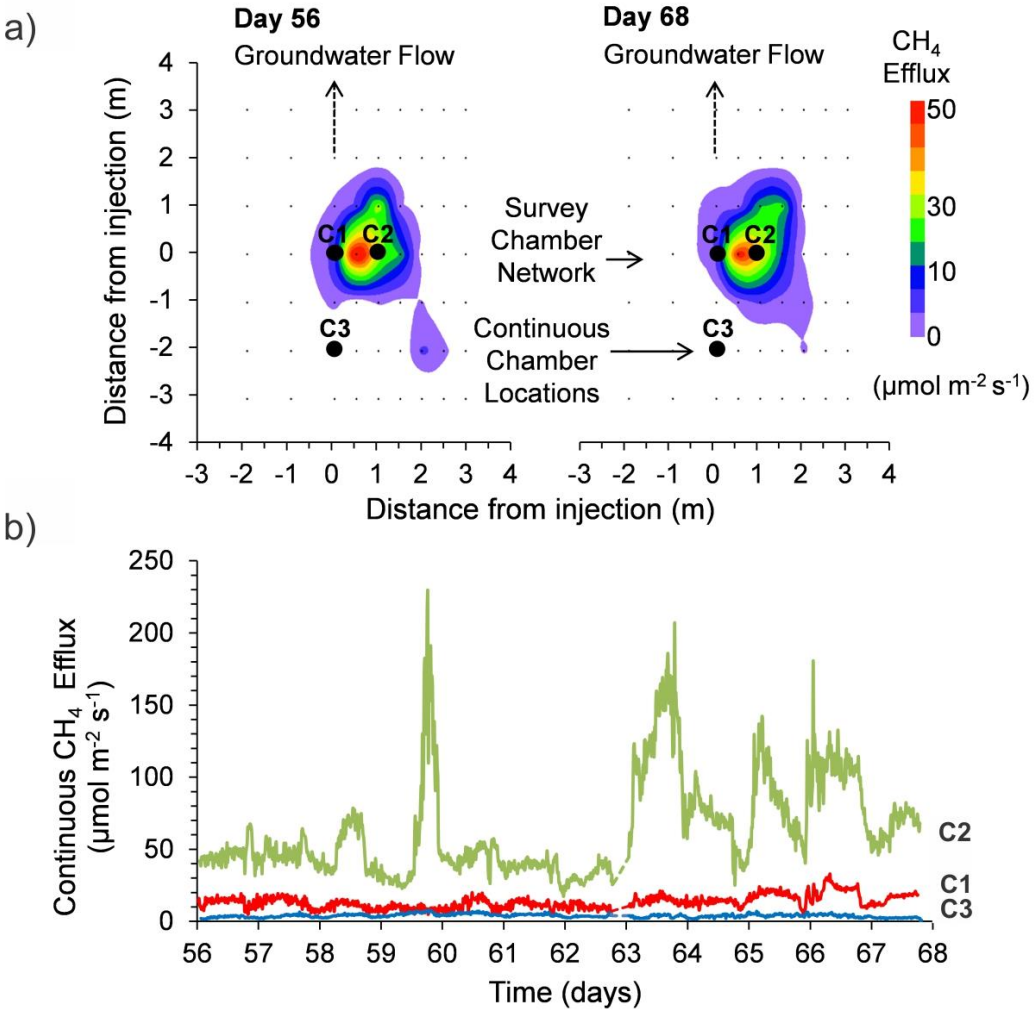

Fig. 3: a) Spatial distribution of methane efflux on days 56 and 68 of the experiment and b) continuous LTCs C1, C2, and C3 provided continuous methane efflux measurements between days 56 and 68.

157 The spatial extent of free gas in groundwater was further investigated using ground-penetrating
158 radar (GPR) to a depth of 5 m. Methane preferentially accumulated within a sequence of
159 horizontally layered and interconnected sand lenses (Extended Data Fig. 6). The maximum GPR
160 response occurred on day 65 (Fig. 4), where despite limited heterogeneity in the aquifer, methane
161 migrated much faster and farther than that predicted by advective groundwater flow; i.e., a lateral
162 extent of >17 m versus an estimate of ~6 m based on aquifer hydraulic properties and
163 gradients[22]. This period of maximum lateral extent was accompanied by a systematic decline in
164 $[CH_4]_{(aq)}$ and P_{TDG} around the injection zone (Fig. 2b, c); here, rapid lateral expansion of free-
165 phase gas in the direction of groundwater flow aided by horizontal bedding, led to a temporary
166 reduction in gas pressure and displacement of CH_4-charged groundwater around the injection.
167 These combined observations suggest vertical buoyancy-driven methane gas migration and/or
168 dissolution into groundwater over a period of days to weeks may influence the lateral extent of
169 free gas migration; however, the time and distance scales will depend on site specific gas leakage
170 rates and subtle variations in aquifer properties. In the case of our shallow unconfined aquifer,
171 known to be relatively homogeneous in the context of single-phase fluid flow, fugitive free-
172 phase methane spread more extensively than presupposed even for relatively low leakage rates
173 and short time scales. Lateral migration will likely be more significant in deeper confined or
174 partially confined aquifers subject to higher real-world leakage rates.

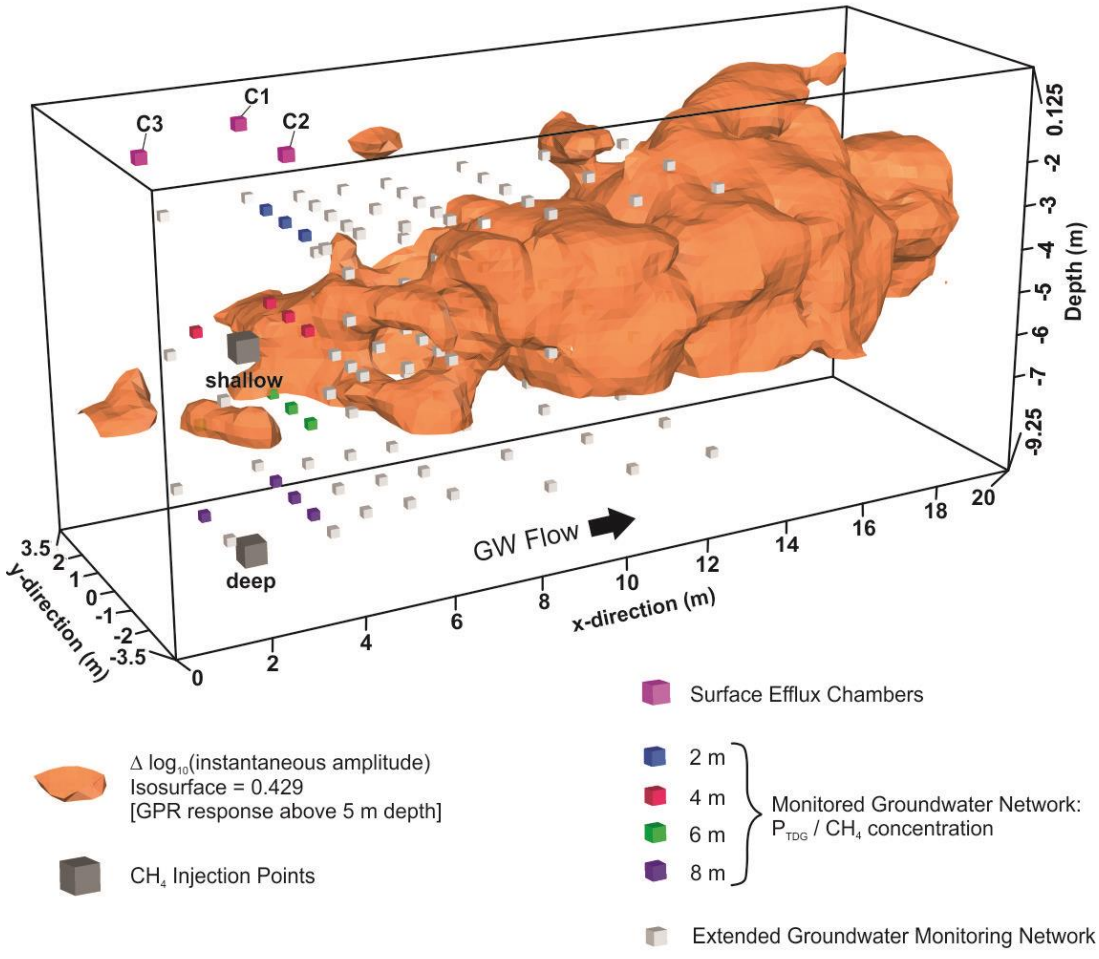

Fig. 4: GPR response associated with free-phase CH_4 methane accumulation (orange) extending downgradient from the injection points. The iso-surface boundary demarcates a laterally extensive volume of high-amplitude reflection events (see Methods and Extended Data Fig. 6), in the direction of groundwater flow from the injection points, impacted by methane gas accumulation beneath and along distinct sedimentary interfaces on day 65.

The potential for microbial attenuation of the released methane was investigated by screening the groundwater for methanotrophic bacteria with 16S rRNA gene amplicon sequencing. Prior to methane injection, methanotrophic microorganisms (e.g., *Methylococcaceae*) were not detected and methylotrophic microorganisms that degrade one-carbon compounds but cannot oxidize methane (e.g., *Methylophilaceae*) constituted <2 % of the overall community and decreased in

abundance with depth (Fig. 5a). Methane release strongly altered the microbial community composition (Fig. 5a) and stimulated growth of both aerobic methanotrophic *Methylococcaceae* and aerobic methylotrophic *Methylophilaceae* despite low oxygen concentrations throughout the aquifer yet in concurrence with the aqueous chemistry evolution previously described (Extended Data Fig. 2). These two clades became the dominant taxa at 2 m and were very abundant at 4 m, with stable or increasing numbers of up to 1.1×10^5 cells·ml^{-1} (Fig. 5b) indicating active populations; their growth also appeared coupled, as noted for oxygen-limited methane oxidation[32, 33]. An increase in the relative abundance of sulfate-reducing bacteria, related to *Peptococcaceae*, indicates that methane release led to anoxic conditions at 6 and 8 m, potentially a result of aerobic methane oxidation. This population shift was associated with a sharp decline in total cell counts at 6 m depth. Taxa capable of the anaerobic oxidation of methane were not detected, which, together with oxygen limitation, explains why microbial methane oxidation was relatively ineffective (Extended Data Fig. 2). However, methane injection strongly and persistently disturbed indigenous microbial communities, with no sign of recovery after 245 days.

During injection, the δ^{13}C values of dissolved methane in groundwater rapidly converged towards the carbon isotope ratio of the injected methane (-42‰). After 245 days, the δ^{13}C-CH_4 remained unchanged and showed little indication of microbial conversion in the saturated groundwater zone (Extended Data Fig. 3). Isotope ratios indicate that methane was not significantly degraded within our monitoring period; more significant degradation, and therefore, potential water quality changes are expected to occur over longer time scales and with varying leakage rates, sediment composition and/or redox conditions.

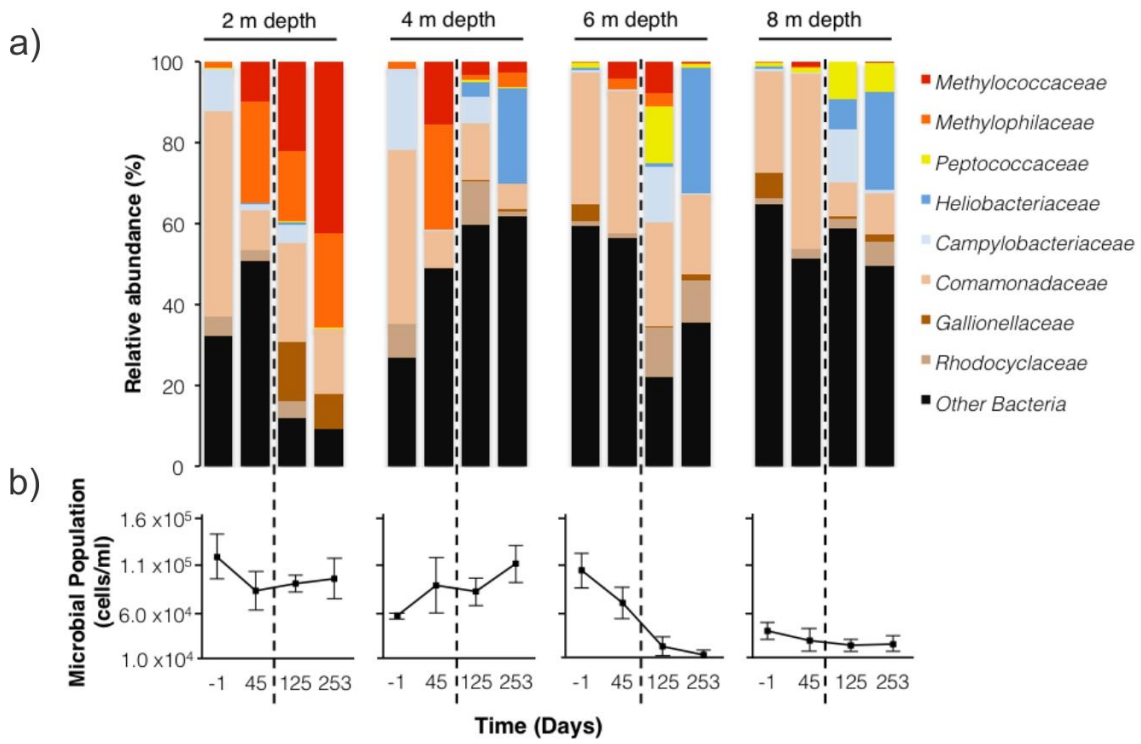

Fig. 5: (a) Relative sequence abundances of bacterial taxa from monitoring well M6 (1 m downgradient of injection zone) determined by 16S rRNA gene amplicon sequencing. Methane was injected from day 0 to 72 (dashed line). Methanotrophs are shown in red, methylotrophs in orange, and sulfate reducers in yellow. Other taxa possibly involved in the cycling of sulfur and iron are shown in blue and brown, respectively. (b) Total microbial cell counts at monitoring well M6 shown as average counts of ten independent microscopic fields; bars show standard deviation.

The behaviour of immiscible-phase liquids and dissolved contaminant plumes in the Borden aquifer has been extensively studied over the past 40 years, particularly hydrodynamic dispersion of solutes in relation to aquifer anisotropy[34, 35, 36]. These studies show solute dispersion is a weak process especially in directions transverse to groundwater flow but exhibits pronounced influence on immiscible liquid flow and distributions. Our experiment shows that subtle variations in aquifer properties can also have a major impact on fugitive methane distribution.

Although the volume of injected methane was relatively conservative (0.17–4.32 $m^3 \cdot day^{-1}$) in

223 comparison to leakage scenarios deemed critical by regulatory agencies (i.e., >300 $m^3 \cdot day^{-1}$)[14],
224 the lateral extent of the impacted groundwater zone relative to the depth of injection was
225 substantial (~4:1), significantly exceeding the observed methane emission footprint at surface.
226 This large impact zone, as indicated by the GPR, was facilitated by small-scale geologic layering
227 with varying permeability, where the horizontal direction represents the orientation of highest
228 permeability. Here, the thin, finer, silty sand layers impeded upward migration of free-gas,
229 thereby trapping and shunting the gas laterally between coarser, more permeable interconnected
230 sand layers, resulting in a hydrodynamically-dispersed plume consisting of free-phase and
231 dissolved methane (Fig 6).

232 Injected methane, as free- and dissolved-phases, persisted in the groundwater throughout the
233 245 day monitoring period. Even a small mass of injected methane over a relatively short period
234 of time (~51 m^3 over 72 days) exceeded the capacity of microbial populations present in the
235 aquifer volume investigated (~600 m^3) to significantly attenuate dissolved methane. This was in
236 contrast to the observed perturbation to the indigenous microbial community in the groundwater
237 zone and more active methane degradation in the thin, aerobic vadose zone.

238 Based on these observations, fugitive methane from a leaky petroleum well casing may have a
239 strong propensity to migrate horizontally in deeper aquifers (Fig. 6). Here, anisotropy would
240 facilitate lateral migration and retention of CH_4 in the groundwater zone, while buoyancy would
241 enhance dispersion and upward migration to the vadose zone. The high mobility of free-phase
242 gas will result in a laterally extensive dispersed methane gas zone extending in the direction of
243 groundwater flow, accompanied with hydrochemical alterations of the groundwater.

244

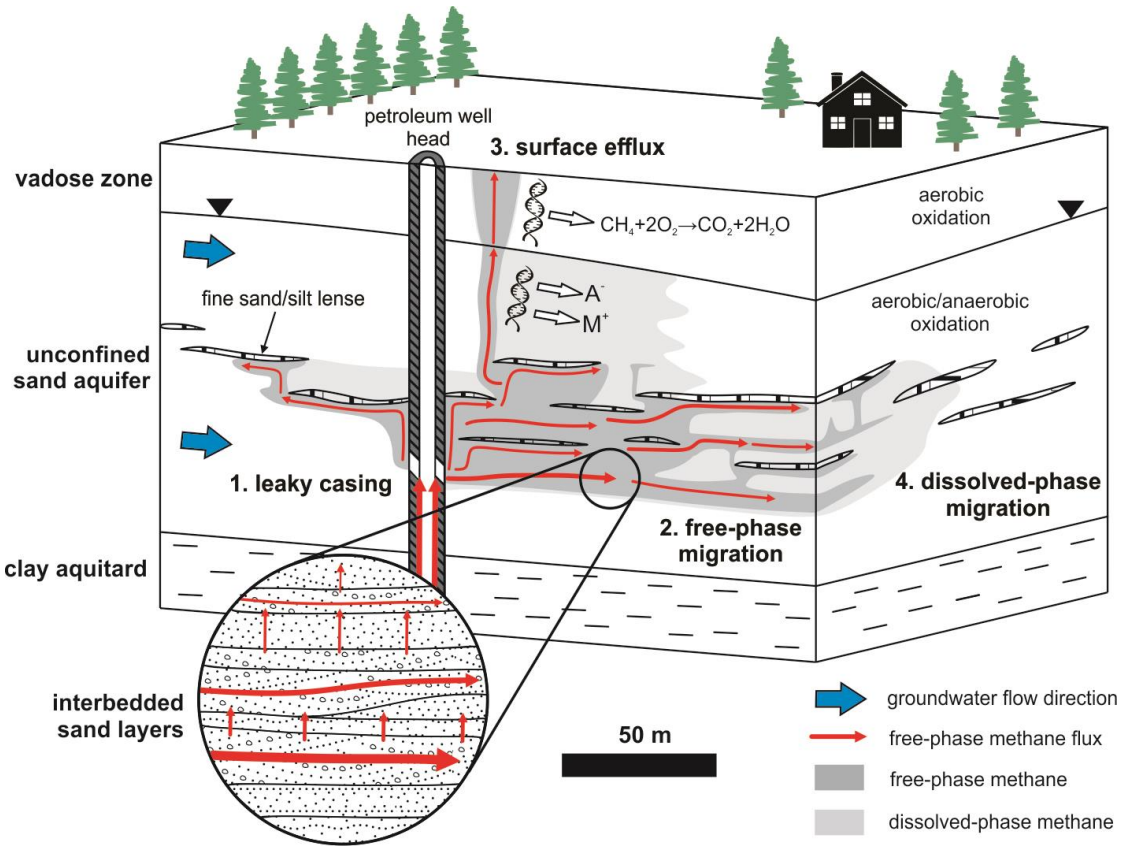

Fig. 6: Conceptual model of a continuous methane leak into a shallow groundwater aquifer: 1) a compromised energy well casing allows release of methane gas; 2) laterally extensive free-phase gas migration controlled by subtle geological variability; 3) variable methane efflux at the surface with potential for explosion risk and greenhouse gas emission; and 4) a temporally persistent dissolved methane plume. Aerobic oxidation of methane occurs in the vadose zone via microbes but degradation is negligible in the saturated zone at early stages.

Most fresh water aquifers overlying sedimentary basins exploited for petroleum resources are more heterogeneous in geological character than the Borden aquifer. In the case of a real leakage event from a shale gas development, we expect fugitive methane to originate from leaks along well bores, and that the gas may enter geologic layers much deeper than the fresh groundwater zone. Nevertheless, methane should be expected to migrate outward primarily along bedding due to anisotropy and eventually upward due to buoyancy. The existence of vertical pressure

gradients in geologically heterogeneous domains indicates that three-dimensional groundwater monitoring networks will be critical for effective characterization of fugitive CH_4 transport and associated geochemical impacts.

Current groundwater monitoring requirements in areas of energy resource development have perceived groundwater impacts to methane leakage as secondary to atmospheric emissions. However, our study shows that gas-phase migration from a high-pressure source in the saturated zone, are an equivalent, if not, more significant process relative to atmospheric emissions. Present-day monitoring efforts do not consider the groundwater resource in its entirety and involve only periodic sampling from existing, sparsely located domestic wells, which serve as receptors at risk, rather than adequate monitors for groundwater resource impact evaluation. Current surface and subsurface monitoring efforts for shale gas development are thus insufficient to meaningfully detect or assess methane impacts to atmosphere and groundwater from below, and/or releases from the groundwater zone into the atmosphere. Indeed, even our high-resolution approach was not adequate to fully capture the temporal and spatial distribution of surface emissions and groundwater impacts, highlighting the need for detailed and innovative surface measurements at shale gas sites.

In the present conventional approach, methane leakage from shale gas wells is assessed by measurements only at the well head without consideration of groundwater quality impacts. Our experimental field results show that surface flux of methane to the atmosphere is not indicative of the lateral extent of methane-induced groundwater quality impacts, of which, should be of equal concern to atmospheric emission. Current efforts by oil and gas companies to locate and mitigate casing vent flow leaks or breaches in casings would identify entry points into the subsurface, and thus, facilitate groundwater impact monitoring strategies. Most importantly, we

demonstrate that meaningful characterization and effective monitoring of fugitive methane in freshwater aquifers can be achieved through a multi-disciplinary and multi-scale monitoring network that intercepts and delineates a fugitive methane contaminant plume emanating from a leaky petroleum well.

References

1. Malakoff, D. The gas surge. *Science* **344**(6191), 1464-1467 (2014)

2. Vidic, R. D., Brantley, S. L., Vandenbossche, J. M., Yoxtheimer, D. & Abad, J.D. Impact of shale gas development on regional water quality. *Science* **340** (6134), (2013)

3. Jackson, R. E., Gorody, A. W., Mayer, B., Roy, J. W., Ryan, M. C. & Van Stempvoort, D. R. Groundwater protection and unconventional gas extraction: the critical need for field-based hydrogeological research. *Ground Water* **51**(4), 488-510 (2013)

4. Dusseault, M. B., Gray, M. N. & Nawrocki, P. A. Why oilwells leak: cement behavior and long-term consequences. Society of Petroleum Engineers International Oil and Gas Conference and Exhibition, Beijing, China, 7-10 November (2000)

5. Dusseault, M., Jackson, R. & MacDonald, D. *Towards a Road Map for Mitigating the Rates and Occurrences of Long-Term Wellbore Leakage.* Special Report: University of Waterloo and Geofirma (2014)

6. Osborn, S. G., Vengosh, A., Warner, N. R. & Jackson, R. B. Methane contamination of drinking water accompanying gas-well drilling and hydraulic fracturing. *PNAS* **108**(20), 8172-8176 (2011)

7. Darrah, T. H., Vengosh, A., Jackson, R. B., Warner, N. R. & Poreda, R. J. Noble gases identify the mechanisms of fugitive gas contamination in drinking-water wells overlying the Marcellus and Barnett Shales. *PNAS* **111**(39), 14076-14081 (2014)

8. Heilweil, V. M., *et al.* Stream measurements locate thermogenic methane fluxes in groundwater discharge in an area of shale-gas development. *Environ. Sci. Technol.* **49**(7), 4057-4065 (2015)

9. Heilweil, V. M., *et al.* A stream-based methane monitoring approach for evaluating groundwater impacts associated with unconventional gas development. *Ground Water* **51**(4), 511-524 (2013)

10. Humez, P. B., *et al.* Occurrence and origin of methane in groundwater in Alberta (Canada): Gas geochemical and isotopic approaches. *Sci Total Environ*. **541,** 1253-1268 (2016)

11. Roy, N., Molson, J., Lemieux, J.-M., Van Stempvoort, A. & Nowamooz, A. Three-dimensional numerical simulations of methane gas migration from decommissioned hydrocarbon production wells into shallow aquifers. *Water Resour. Res.* **52**(7), 5598-5618 (2016)

12. Royal Society. *Shale Gas Extraction in the UK: A Review of Hydraulic Fracturing*. The Royal Society and The Royal Academy of Engineering, Issued: June 2012 DES2597 (2012)

13. Council of Canadian Academies. *Environmental Impacts of Shale Gas Extraction in Canada*. The Expert Panel on Harnessing Science and Technology to Understand the Environmental Impacts of Shale Gas Extraction, Council of Canadian Academies, Ottawa, Ontario (2014)

14. Nowamooz, A., Lemieux, J. M., Molson, J. & Therrien, R. Numerical investigation of methane and formation fluid leakage along the casing of a decommissioned shale gas well. *Water Resour. Res.* **51**(6), 4592-4622 (2015)

15. Ingraffea, A. R., Wells, M. T., Santoro, R. L. & Shonkoff, S. B. C. Assessment and risk analysis of casing and cement impairment in oil and gas wells in Pennsylvania, 2000-2012. Proc. *Natl. Acad. Sci. U.S.A.* **111**(30), 10955-10960 (2014)

16. Caulton, D. R. *et al*. Toward a better understanding and quantification of methane emissions from shale gas development. *Natl. Acad. Sci. U.S.A.* **111**(17), 6237-6242 (2014)

17. Jackson, R. B., *et al.* Increased stray gas abundance in a subset of drinking water wells near Marcellus shale gas extraction. *PNAS* **110**(28), 11250-11255 (2013)

18. Molofsky, L. J., Connor, J.A., Wylie, A. S., Wagner, T. & Farhat, S.K. Evaluation of methane sources in groundwater in northeastern Pennsylvania. *Ground Water*, **51**(3), 333-349 (2013)

19. Jackson, R. E. & Heagle, D. J. Sampling domestic/farm wells for baseline groundwater quality and fugitive gas. *Hydrogeol. J.* **24**(2), 269-272 (2016)

20. Siegel, D. I., Azzolina, N. A., Smith, B. J., Perry, A. E. & Bothun, R. L. Methane concentrations in water wells unrelated to proximity to existing oil and gas wells in northeastern Pennsylvania. *Environ. Sci. Technol.*, **49**(7), 4106-4112 (2015)

21. Parker, B. L., Cherry, J. A. & Chapman, S. W. Discrete fracture network approach for studying contamination in fractured rock. *AQUA mundi*. Am06052, 101-116 (2012)

22. Cherry, J. A., Gillham, G. W., Anderson, E. G. & Johnson, P. E. Migration of contaminants in groundwater at a landfill - A case study. 2. Groundwater monitoring devices. *J. Hydrol.* **63**(1-2), 31-49 (1983)

23. Sudicky, E. A. & Illman, W. A. Lessons learned from a suite of CFB Borden experiments. *Ground Water*, **49**(5), 630-648 (2011)

24. Tomlinson, D. W., Thomson, N. R., Johnson, R. L. & Redman, J. D. Air distribution in the Borden aquifer during in situ air sparging. J. Contam. Hydrol. 67(1-4), 113-132 (2003)

25. Cahill, A. G., Marker, P. & Jakobsen, R. Hydrogeochemical and mineralogical effects of sustained CO2 contamination in a shallow sandy aquifer: A field-scale controlled release experiment. *Water Resour. Res.* **50**(2), 1735-1755 (2014)

26. Manning, A. H., Kip Solomon, D. & Sheldon, A. L. Applications of a total dissolved gas pressure probe in ground water studies. *Ground Water* **41**(4), 440-448 (2003)

27. Eltschlager, K. K., Hawkins, J. W., Ehler, C. & Baldassare, F. *Technical Measures for the Investigation and Mitigation of Fugitive Methane Hazards in Areas of Coal Mining.* Office of Surface Mining Reclamation and Enforcement Appalachian Regional Coordinating Center Pittsburgh, PA (2001)

28. Thomson, N. R. & Johnson, R. L. Air distribution during in situ air sparging: an overview of mathematical modeling. *J. Hazar. Mater.* **72**(2-3), 265-282 (2000)

29. McCray, J. E. Mathematical modeling of air sparging for subsurface remediation: state of the art. *J. Hazar. Mater.* **72**(2-3), 237-263 (2000)

30. Johnson, P. C., Das, A. & Bruce, C. Effect of flow rate changes and pulsing on the treatment of source zones by in situ air sparging. *Environ. Sci. Technol.* **33**(10), 1726-1731 (1999)

31. Cahill, A. G., Jakobsen, R., Mathiesen, T. B. & Jensen, C. K. Risks attributable to water quality changes in shallow potable aquifers from geologic carbon sequestration leakage into sediments of variable carbonate content. *Int. J. Greenhouse Gas Control.* **19**, 117-125 (2013)

32. Beck, D. A. C. *et al.* A metagenomic insight into freshwater methane-utilizing communities and evidence for cooperation between the Methylococcaceae and the Methylophilaceae. *PeerJ* **1**, e23 (2013)

33. Oshkin, I. Y., *et al.* Methane-fed microbial microcosms show differential community dynamics and pinpoint taxa involved in communal response. *ISME J* **9**, 1119-1129 (2015)

34. Sudicky, E. A. A natural gradient experiment on solute transport in a sand aquifer: spatial variability of hydraulic conductivity and its role in the dispersion process. *Water Resour. Res.* **22**(13), 2069-2082 (1986)

35. Frind, E. O. & Hokkanen, G. E. Simulation of the Borden plume using the alternating direction Galerkin Technique. *Water Resour. Res.* **23**(5), 918-930 (1987)

36. Sudicky, E. A., Cherry, J. A. & Frind, E. O. Migration of contaminants in groundwater at a landfill – A case study. *J. Hydrol.* 63(1-2), 81-108 (1983)

Methods

Injection System Configuration and Methodology

The gas delivery system was composed of two, 45° inclined sparging wells emplaced at 4.5 and 9 m depths (termed shallow and deep). Each sparging well was constructed using a 1 m length of porous polyethylene (PE) well screen (SCHUMASOIL®) connected to a mass flow controller and two canisters (master and slave) of industrial grade methane by PE tubing. Injection screens were installed using a Geoprobe (model 7822DT) direct push system in a vertical plane perpendicular to groundwater flow. Borden sediment is not freestanding following use of a Geoprobe direct push tool; drilled holes collapse almost immediately following removal of drill rods. Angled injection wells were used to minimize migration of methane along the delivery tube whilst maximizing gas release into the aquifer. Injection wells were connected to a control unit containing two individual (shallow and deep) mass flow controllers (Red-y smart GSC-C9SA-BB26) controlled by associated software (Get Red-y, Vögtlin Instruments AG, Switzerland).

Gas injection was conducted in four phases at three rates as shown in Extended Data Table 1. Total gas volume injected during the experiment was 51,350 L of industrial grade methane (34.9 kg at 1.013 bar and 15 °C). Following injection, gas delivery wells were sealed by non-return valves to prevent immediate flow back.

Aqueous Chemistry Sampling

Groundwater samples were collected through 32 multilevel groundwater sampling systems (M1 – M32) comprising a total of 112 depth-discrete sample points (Fig. 1b). Sampling systems were constructed using 6 mm PE tubing connected to 5 cm length geotextile covered screens (Nitex monofilament screen cloth, 200 micron mesh) fixed at multiple depths to a single polyvinyl

chloride (PVC) center-stock. Multi-level systems were instrumented with three screens (2-, 5-, and 8-m depths), four screens (2-, 4-, 6-, and 8-m depths), or five screens (2-, 3-, 4-, 5-, and 6-m depths) depending on the location and proximity to the injection point. The groundwater monitoring network covered an area of approximately 72 m^2, spanning 10 m downgradient of the injection zone. Multi-levels were installed using a Geoprobe (model 7822DT) direct push system at higher density around and immediately downgradient of the injection zone at required depths. A plan view of the groundwater multi-level network sample points is shown in Fig. 1b.

Physical chemistry parameters including electrical conductivity (accuracy 1 µS/cm), pH (accuracy 0.02), and total dissolved gas pressure (1 mmHg) were measured with a multi-parameter water quality sonde and flow-through cell (Manta 2, Eureka Water Probes, Austin, TX) using a peristaltic pump at constant, low flow rate (approximately 40 $mL \cdot min^{-1}$). Dissolved gas samples were collected by filling either biocide-treated pre-evacuated 125 mL glass vials or 40 mL VOA vials, submerged in a beaker and piercing or sealing with a septa cap, respectively (leaving no headspace). Samples were stored upside down at 4 °C and measured on a Bruker 450 Natural Gas Analyzer for dissolved hydrocarbons (C_1-C_3) and other dissolved gases within 7 days. Major and minor cation concentrations were determined following filtration (0.45 µm cellulose acetate filters) and acidification for cation samples (concentrated HNO_3) by ion chromatography or inductively coupled plasma-mass spectrometry (ICP-MS; PerkinElmer Elan 6100DRC). Accuracy of ICP-MS measurements are 5% with limits of detection ($mmol \cdot L^{-1}$) for parameters shown as follows: Al, 1.11; Ba, 0.14; Ca, 3.74; Fe, 0.89; K, 1.27; Mg, 0.82; Mn, 0.036; Na, 2.17; Si, 3.55; Sr, 0.03; and Zn, 0.15. Alkalinity was determined (by Gran titration) for selected samples.

Experimental Field Site

The experimental site was characterized hydro-geochemically prior to methane injection through a series of depth discrete background samples (three sampling events over 4 months prior to methane injection). The presence of a historic construction waste based landfill leachate plume at the base of the aquifer (i.e., 8-9 m depth)[37] led to the formation of two distinct aqueous chemistries. The upper zone, from the water table down to approximately 6-7 m depth, features sub-oxic groundwater (i.e., negative Eh with low to no dissolved O_2) with moderate total dissolved solids (TDS; 250-450 $mg \cdot L^{-1}$) and electrical conductivity (EC; 400-600 $\mu S \cdot cm^{-1}$) in the Fe/Mn reduction stage of the redox sequence and which is not currently impacted by landfill leachate. At 8 m depth, landfill leachate impacts the groundwater chemistry as evidenced by a significant increase in TDS (1100-1500 $mg \cdot L^{-1}$) and EC (1800-2000 $\mu S \cdot cm^{-1}$) caused primarily by increases in concentrations of major ions and alkalinity. Concentrations of dissolved methane are naturally low (0.02-0.2 $mg \cdot L^{-1}$), the methane is of biogenic origin ($\delta^{13}C\text{-}CH_4$ as low as -80 ‰), and $\delta^{13}C\text{-}CH_4$ values occasionally as high as -48 ‰ suggest some occurrence of methane oxidation in the aquifer. Total dissolved gas pressure (P_{TDG}) is variable across the site, ranging from 700 to 860 mmHg (standard deviation 40-50 mm Hg). Mean aqueous chemical conditions from three background (BG) samples taken 50, 21, and 2 days prior to injection are shown in Extended Data Table 2. The water table at the experimental site was approximately 1 m below ground surface (bgs) during the duration of the experiment, varying ± 0.5 m from spring to fall, respectively.

Geophysical Data Collection and Data Processing

Ground-penetrating radar (GPR) measurements were collected using a PulseEKKO 100 GPR system (Sensors & Software, Mississauga, Canada) equipped with 200 MHz bistatic antennas and a 1000 V transmitter. Reflection profiles were acquired along a series of parallel 20 m long

lines spaced 0.5 m apart, and orientated parallel to groundwater flow direction; these lines were connected by orthogonal tie lines positioned at 0.5, 8.5, 12, 15, and 18 m downgradient (Fig. 1c). Radar traces were recorded using a spatial step-size of 0.1 m with the antennas spaced 1 m apart and orientated perpendicular to the survey line direction. A 64-trace stack was used with a temporal sampling interval of 800 ps. Data were recorded using a manual trigger and measuring tapes.

Post-acquisition processing and visualization were performed using ReflexW (v.7) (Sandmeier Software, Germany). The processing flow consisted of a high-pass mean dewow filter to remove DC shifts on individual traces; zero-time corrections; a fixed gain function to compensate for attenuation; a bandpass frequency filter (25-75-250-325 MHz); a notch frequency filter (40-85-85-125 MHz) to suppress ringing (e.g., near surface efflux chambers and electrical wires); and a three-trace horizontal filter. The instantaneous amplitude – a complex trace attribute that removes the effects of wavelet polarity and phase[38] – was calculated to more accurately measure changes in reflection strength through the injection period. Here, the instantaneous amplitude provided a measure of changes in the dielectric contrast along closely spaced beddings planes. The high dielectric constant of water ($\kappa = 81$) relative to mineral grains ($\kappa = 4 - 6$) and air/gas ($\kappa = 1$)[39] results in a high reflection coefficient at the interface between contrasting stratigraphic units. In this study, the vertical and lateral migration of free-phase methane within the sand aquifer will be impeded at interfaces demarcating subtle changes in capillary properties. Subsequent accumulation of methane gas along these capillary boundaries will lead to a reduction in water saturation just below the interface as gas displaces water; this gas will continue to desaturate the pore space until the capillary pressure exceeds the air-entry pressure of the overlying sediment, upon which the gas will pass through[40]. Spatiotemporal GPR amplitude

variations along sedimentary interfaces in the radar profiles were used to assess gas accumulation along stratigraphic bedding planes (Extended Data Fig. 6).

The spatial distribution of energy (i.e., instantaneous amplitude) was calculated over a 20 × 7 m area using the reflection profiles shown in Fig. 1c. A 3D cube (20 × 7 × 6 m) of the instantaneous amplitude was computed using an inverse distance weighting method based on a uniformly discretized 0.25 (x, y, z) grid, assuming a fixed radar velocity of 0.06 $m \cdot ns^{-1}$ [24].

Surficial Efflux Monitoring Methods

Methane emissions to the atmosphere were estimated by measuring methane soil gas effluxes throughout the experiment. Continuous effluxes were monitored with long-term LI-COR chambers (LI-8100-104) connected to a LI-COR Multiplexer (LI-8150) (LI-COR Inc., Lincoln, NE, USA), cavity ring down laser spectroscopy (CRDS), and extended range, Ultraportable Greenhouse Gas Analyzer (UGGA) (Los Gatos Research (LGR), Mountain View, CA, USA). The spatial distribution of gas effluxes was measured with a portable LI-COR chamber (LI-8100-103) connected to the UGGA[41].

Flux measurements were completed by placing chambers on PVC collars (0.2 m ID) inserted into the soil prior to commencing injection. The portable chamber was used in a 5 × 6 m grid and three long-term chambers (LTCs) were placed directly above (Chamber 1) and offset by 1-2 m (Chambers 2 and 3) of the methane injection (Extended Data Fig. 4). All chamber measurements lasted 3 min and an automated cycle switched between chambers every 10 min. Effluxes were calculated and are reported for selected times in $\mu mol \cdot m^{-2} \cdot s^{-1}$ (LI-COR, 2015).

Stable Carbon Isotope Ratio Measurements

Multi-level soil gas monitoring wells were installed (Extended Data Fig. 4) for periodic collection of soil gas samples and subsequent stable carbon isotope ($\delta^{13}C$) ratio analyses of methane and CO_2. Ports were installed at depths of 10, 30, and 50 cm. Wells were constructed of 1/8" gas impermeable tubing with mesh screens at the bottom and gas-tight fitting and septa at the top. Samples were collected with gas tight syringes (Valco Instruments Co. Inc., Brockville, ON, Canada) and stored in pre-evacuated 12 mL vials (Labco Limited, Lampeter, Ceredigion, UK). Gas samples for isotope analyses were transferred directly using a gas-tight syringe (CH_4 >3000 ppmv) or via a pre-concentration device (CH_4 <3000 ppmv) into a Thermo Scientific Trace GC Ultra where methane was isolated and subsequently quantitatively converted to CO_2 at 1000 °C using a GC-Isolink. The CO_2 was subsequently introduced into a Thermo Finnigan MAT253 isotope ratio mass spectrometer via a Conflo IV system, and carbon isotope ratios of methane were determined in continuous flow mode. Carbon isotope ratios of methane are reported in the standard delta notation (‰) relative to V-PDB with a precision of better than ± 0.5‰. $\delta^{13}C$ values of CO_2 were determined with the same system with a precision of better than ± 0.3‰.

Mass Balance Calculations

Mass balance calculations were conducted based on survey chamber measurements at selected times and making use of LTC data for specified time intervals. Here, we present mass balance calculations from the time interval ranging from 56 to 68 days (Δt = 11.75 days), for which near-continuous long-term measurement data from three LTCs were available (see Fig. 3b). In addition, we present survey efflux data from days 56 and 68 (see Fig. 3a) when complete sets of survey measurements were conducted at all monitoring locations showing methane above atmospheric levels. Survey measurements were also used to assess the extent and magnitude of

effluxes within and outside of the area covered by the LTCs. Based on the survey measurements, the rate of methane loss to the atmosphere was estimated using

$$R_s(t) = \sum_{i=1}^{N_s} J_i^s(t) A_i^s,$$

where $R_s(t)$ is the rate of methane loss to the atmosphere (μmol·s^{-1}) obtained from survey measurements at time t; $J_i^s(t)$ is the measured methane efflux at time t and survey chamber location i (μmol·m^{-2}·s^{-1}); A_i^s is the area assigned to survey chamber location i for mass balance calculations (m^2); and N_s is the number of survey chamber locations.

Survey measurements were conducted over a period of several hours; however, for the purpose of the mass balance calculation it was assumed the measurements are temporally co-located and are representative of the time period of the measurements during a specific day. Extended Data Table 4 shows the results of the mass balance calculations based on survey chamber data for days 56 and 68 in relation to the injection rate.

This analysis suggests a mass loss of injected methane to the atmosphere in excess of 20%. When interpreting these data, the methane effluxes show strong temporal variations so it is therefore essential to also include measurements from the LTCs in the mass balance calculations despite their relatively low spatial resolution. Visual examination of the survey results demonstrates that the highest effluxes were spatially co-located with the LTCs (see Fig. 3a). A quantitative assessment of the survey chamber data for days 56 and 68 (Table 2) confirms that most of the total efflux occurred within the area covered by the LTCs (>98%).

Mass balance calculations for methane loss to the atmosphere can therefore also be evaluated based on the LTC data, accounting for temporal variability of the fluxes. The mass balance can

be further amended by survey chamber data for the area outside of the LTC measurements. Using this approach, the average rate of methane loss to the atmosphere from the area associated with the LTCs over a specified time period ΔT (s) was estimated using

$$R_{l,avg} = \frac{1}{\Delta T} \sum_{i=1}^{N_l} \sum_{j=1}^{N_i} \Delta t_{ij} J_{ij}^{l} A_i^{l} \,,$$

where $R_{l,avg}$ is the average rate of methane loss to the atmosphere (μmol·s^{-1}) obtained from LTC measurements during time period ΔT; J_{ij}^{l} is the measured methane efflux at LTC location i during time interval j (μmol·m^{-2}·s^{-1}); A_i^{l} is the area assigned to LTC location i for mass balance calculations (m^2); Δt_{ij} is the time interval j for LTC i (s); $N_l$is the number of LTCs; and N_i is the number of measurements for LTC i during time period ΔT.

The total rate of mass loss accounting for fluxes from the LTCs and survey chambers outside the long-term monitoring grid was calculated using

$$R_{tot} = R_{l,avg} + R_{s,avg}^{ext},$$

where R_{tot} is the total average rate of mass loss to atmosphere over time interval ΔT and $R_{s,avg}^{ext}$ is the average rate of mass loss outside the LTC grid based on survey chamber data.

The average rate of mass loss to the atmosphere between day 56 and 68 (ΔT = 11.75 days), cumulative mass loss during this time period, and fraction of mass lost in comparison to the injected methane are summarized in Extended Data Table 3. These calculations indicate that the mass loss to the atmosphere amounts to 31% of the methane injected over this period of time. These estimates (Extended Data Tables 3-5) are similar, with a difference of approximately 10%. The higher fraction of methane loss to the atmosphere predicted from the LTC data is likely due to the fact that the long-term measurements episodically capture the peak effluxes, which are not

accounted for in the survey data for days 56 and 68 (see Fig. 2). The estimate from the LTC data is therefore considered more representative of site conditions. However, taking into consideration that the calculations neglect the role of methane oxidation in the vadose zone, both mass loss estimates are considered conservative. Methane oxidation in the soil zone likely plays a significant role as indicated by soil gas carbon isotope data.

Microbiological Methods

Sample Filtration

Groundwater from the Borden aquifer for DNA analyses was collected in 1 L Nalgene HDPE bottles, which were completely filled and shipped in iced coolers to the Energy Bioengineering and Geomicrobiology laboratories at the University of Calgary. Upon arrival (5-7 days after sampling), a 250 mL aliquot of each sample was filtered through a 0.22 µm GTTP Isopore membrane filter (Merck Millipore, Cork, Ireland) attached to a sterile 500 mL polysulfone bottle top filter holder (Nalgene). The supernatant was collected in sterile 250 mL Schott bottles and subsequently filtered through a 0.1 µm Supor-100 membrane filter (Pall Corp, Michigan, USA). The filters were stored at -20 °C until DNA extraction.

Microbial Cell Numbers

Unfiltered groundwater (5 mL) was fixed with sterile formaldehyde (final concentration, 4 % v/v) and filtered through a sterile 0.1 µm Merck Millipore VCTP membrane filter. Cell counts from well M6 were performed using a DAPI stain[42] and fluorescence microscopy. Direct cell counts were performed and averaged for 10 fields of view.

DNA Isolation and Quantification

The 0.22 and 0.1 µm filters from each sample were cut into thin strips with a sterile scalpel and transferred in duplicate into autoclaved 2 mL bead beating tubes. Each tube contained 0.5 g of 0.1 mm and 0.5 g of 2.5 mm zirconia-silica beads (BioSpec Products, Bartlesville, OK, USA). High molecular weight DNA was extracted from each filter using an SDS-Chloroform protocol as follows. First, 300 µL each of 0.1 M phosphate buffer (pH 8), 10% SDS lysis buffer (pH 8), and 24:1 chloroform:isoamyl alcohol solution were added in sequence to the tubes. The tubes were loaded onto a bead mill homogenizer (Bead Ruptor 24, Omni Inc, USA) for 45 s at speed setting 5.5. The tubes were centrifuged at 20,000 × *g* for 5 min and the supernatant transferred to a sterile 1.5 mL microcentrifuge tube. Ammonium acetate (7 $mol \cdot L^{-1}$) was then added to achieve a final concentration of 2.5 M. The 1.5 mL tubes were inverted gently by hand for 10 s and centrifuged at 20,000 × *g* for 7 min. The supernatant was transferred into a new sterile 1.5 mL microcentrifuge tube to which 0.54 mL of 100 % isopropanol was added, then stored at -20 °C overnight for DNA precipitation. DNA was pelleted by centrifugation at 4 °C for 30 min. The isopropanol was decanted off and the tubes dried inside a biosafety cabinet for up to 2 h. The DNA in each set of duplicate tubes was re-suspended and pooled by dissolving the pellet in 30 µL of sterile nuclease-free water. DNA quantification was performed with a Qubit 2.0 Fluorometer (Thermo Fischer Scientific). DNA samples were stored at -20 °C. The constitution of 10% SDS lysis buffer (100 ml) was as follows: 48 mL MilliQ water, 2 mL of 5 M sodium chloride, 50 mL Tris solution (pH 8), and 10 g SDS. With the exception of isopropanol and chloroform-isoamyl alcohol solution, all reagents were filter-sterilized with a 0.22 µm syringe filter.

DNA amplification and Illumina 16S rDNA Amplicon Sequencing

The V3-V4 region of 16S rDNA was amplified in a single-step PCR using a KAPA HiFi HotStart reaction kit and primers Pro341F/Pro805R targeting all prokaryotes[43] and including Illumina adapters (Illumina Inc. San Diego CA, USA). The primers were complementary to standard Illumina forward and reverse primers. The reverse primer also contained a 6-bp indexing sequence. PCR reaction conditions for DNA amplification were as follows: initial denaturation at 95 °C for 3 min, followed by 32 cycles of 95 °C for 30 s, 55 °C for 45 s, and 72 °C for 60 s, followed by a final step of 72 °C for 5 min. The amplicon products of triplicate PCR reactions were pooled and purified using AMPure XP beads (Agencourt Bioscience, Beverly, MA, USA). DNA amplicon libraries were prepared from purified DNA using a Nextera XT DNA Sample Prep Kit with Nextera XT Index Kit (Illumina Inc.) as per the manufacturer's instructions. PCR conditions were as follows: 95 °C for 3 min, followed by 10 cycles of 9 °C for 30 s, 5 °C for 45 s, and 72 °C for 60 s, and a final step of 72 °C for 5 min. PCR products were purified with AMPure XP beads and quantified with a Qubit 2.0 Fluorometer. Amplicon libraries were normalized to 2 nM, pooled in equal volumes, denatured in 0.2 N NaOH, and diluted with hybridization buffer according to Nextera XT protocol. Paired-end sequencing (300 × 300 bp) of libraries at 15 pM final concentration was performed on an Illumina Miseq instrument using manufacturer's reagents and according to the manufacturer's instructions.

Analyses of 16S rDNA amplicon data

Paired end reads (300 × 300 bp) were merged with usearch (3) ("-fastq_mergepairs -fastqminovlen 100 -fastqmaxdiffs 8 -fastq_allowmergestagger -fastq_truncqual 3"), followed by trimming of primers with Mothur [44] ("trim.seqs pdiffs=0") and read quality control with usearch ("-fastq_filter -fastq_trunclength 350 -fastq_maxee 1"). Dereplication, removal of singleton and/or chimeric reads, and clustering was done with the uparse pipeline based on 97% sequence

identity[45, 46]. Taxonomic assignment was done with the RDP classifier implemented in Mothur with the SILVA training dataset as the template (http://www.mothur.org/wiki/Taxonomy_outline). Our approach is available online at http://ebg.ucalgary.ca/metaamp.

References:

37. MacFarlane, D. S., Cherry, J. A., Gillham, R. W. & Sudicky, E. A. Migration of contaminants in groundwater at a landfill: a case study: 1. Groundwater flow and plume delineation. *J. Hydrol.* **63**(1–2), 1-29 (1983)

38. Sheriff, R. E. & Geldart, L. P. *Exploration Seismology*. Cambridge University Press: Cambridge, UK (1995)

39. Cassidy, N. J. Electrical and magnetic properties of rocks, soils and fluids. Pages 41-72 in (Ed.) H.M. Jol, *Ground Penetrating Radar: Theory and Applications*. Elsevier: Amesterdam, The Netherlands (2009)

40. Thomson, N. R. & Johnson, R. L. Air distribution during in situ air sparging: an overview of mathematical modeling. *J. Hazar. Mat.* **72**(2-3), 265-282 (2000)

41. Porter, K. G. & Feig, Y. S. The use of DAPI for identifying and counting aquatic microflora. *Limnol. Oceanogr.* **25,** 943-948 (1980)

42. Sihota, N. J., Mayer, K. U., Toso, M. A. & Atwater, J. F. Methane emissions and contaminant degradation rates at sites affected by accidental releases of denatured fuel-grade ethanol. *J. Contam. Hydrol.* **151**, 1-15 (2013)

43. Takahashi, S., Tomita, J., Nishioka, K., Hisada, T. & Nishijima, M. Development of a prokaryotic universal primer for simultaneous analysis of bacteria and archaea using next-generation sequencing. *Plos One* **9**(8), e105592 (2014)

44. Schloss, P. D., *et al.* Introducing mothur: open-source, platform-independent, community-supported software for describing and comparing microbial communities. *Appl. Environ. Microbiol.* **75**(23), 7537-7541 (2009)

45. Edgar, R. C. Search and clustering orders of magnitude faster than BLAST. *Bioinformatics* **26**(19), 2460-2461 (2010)

46. Edgar, R. C. UPARSE: highly accurate OTU sequences from microbial amplicon reads. *Nat. Methods* **10**(10), 996-998 (2013)

Acknowledgments

We acknowledge funding from the Natural Sciences and Engineering Research Council of Canada (NSERC), Strategic Project Grant no. 463045-14. Special thanks for field assistance are given to A. Haggman, B. Ladd, D. Klazinga, T. Cheung, A. Verdin, R. Ingleton, and P. Johnson. Data used in concluding this study are included in the supplementary materials. DNA sequence data are available in the NCBI database (www.ncbi.nlm.gov/) (SRA accession SRP076566, Bioproject accession: PRJNA32558).

Author Contributions AGC, BLP, and JAC conceived, designed, installed, and oversaw the experiment. AGC, CMS, OF, OK and ER collected and processed all field data. All authors interpreted the multi-disciplinary datasets. AGC, BLP, JAC, and CMS generated the first draft of the manuscript before all authors contributed to refinement and finalization.

Author Information

Reprints and permissions information is available at www.nature.com/reprints. The authors declare no competing financial interests. Readers are welcome to comment on the online version of the paper. Correspondence and requests for materials should be addressed to B.L. Parker (bparker@uoguelph.ca).

Extended Data

Extended Data Table 1: Injection phases and rates of industrial grade methane at surface conditions.

Phase	Duration	Shallow Injection Rate	Deep Injection Rate	Total Rate
	days	$L \cdot min^{-1}$	$L \cdot min^{-1}$	$L \cdot day^{-1}$
I	28	0.06	0.06	172.8
II	40	0.35	0.35	1008
III	2	0	0.35	504
IV	2	1.5	1.5	4320

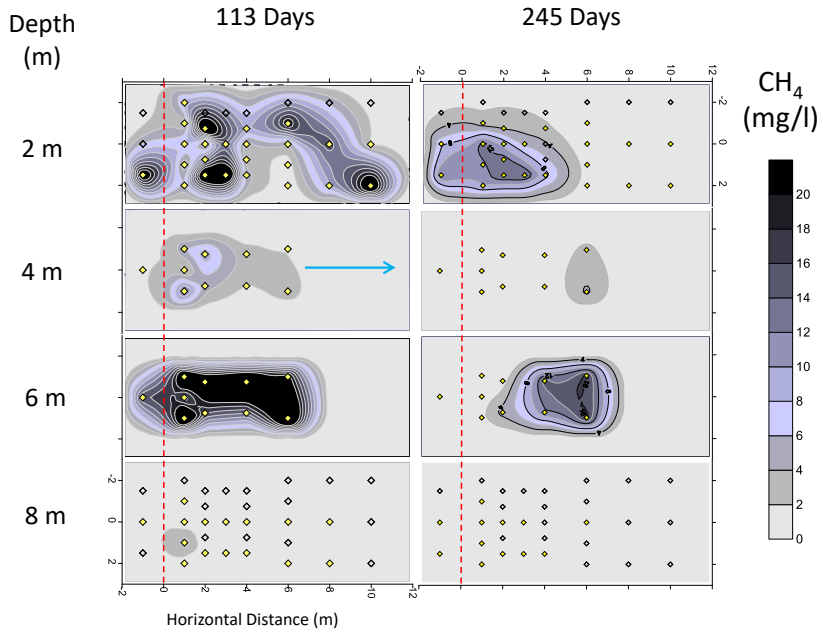

Extended Data Fig. 1: Depth discrete plan view of $[CH_4]_{(aq)}$ contours at 113 days (greatest areal impact) and at 245 days showing capillary barrier control of migration and persistence of methane. Red dashed line indicates methane injection horizon. Blue arrow indicates direction of groundwater flow. Diamonds represent sample points at each depth plane with yellow-filled symbols measured at each time period.

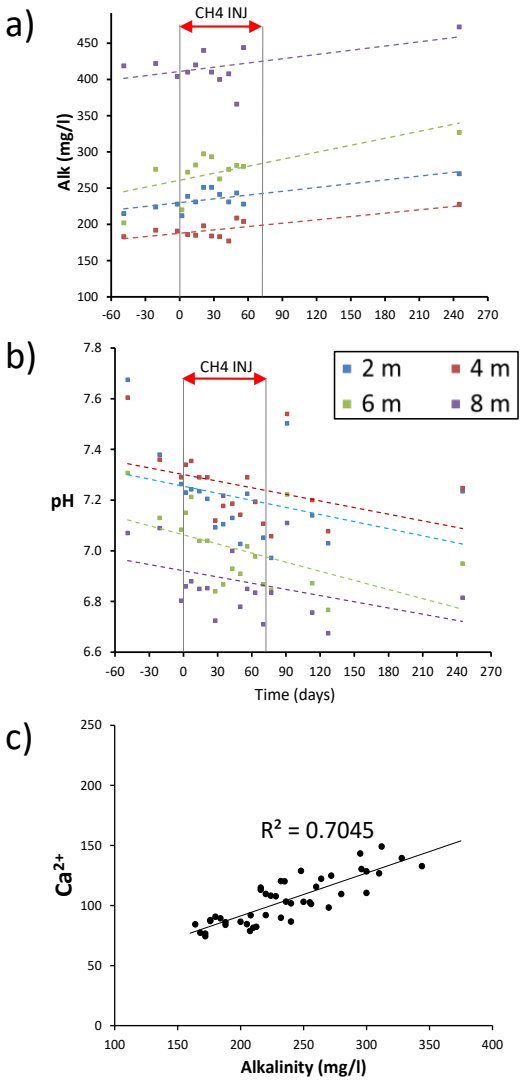

684

685 Extended Data Figure 2: a) Depth discrete average alkalinity around the injection zone (sample
686 points M2, 5, 6 and 7) with time; b) depth discrete evolution of pH around the injection zone
687 (typified by sample point M7) and; c) concentration of Ca^{2+} ($mg \cdot .L^{-1}$) versus alkalinity around
688 the injection zone (sample points M2, 5, 6 and 7). The increasing trend in alkalinity, decreasing
689 trend in pH and positive correlation of Ca^{2+} with alkalinity suggests limited aerobic methane
690 oxidation is occurring, causing weak acidification and dissolution of carbonates. Such processes
691 are known to induce release of trace metals via dissolution and/or ion exchange processes.

Extended Data Table 2: Depth discrete average water chemistry across the monitoring network for background (BG, sample number in brackets) and around the injection horizon (i.e., monitoring points M2, 5, 6, and 7; therefore each depth discrete average is from four samples) at day 245. All concentrations in µmol·L^{-1} except Ca, Cl, and SO_4^{2-} in mmol·L^{-1} and alkalinity in meq·L^{-1}.

Depth (m)	Time	Al	As	Ba	Ca	Fe	K	Mg	Mn	Ni	Si	Sr	Zn	Alk	Cl	SO_4^{2-}	pH
2	BG (55)	0.23	0.002	0.106	2.24	61.6	16.6	179	4.6	0.01	158.1	1.3	0.57	3.8	0.037	0.027	7.4
	254 days	6.74	0.009	0.181	2.47	56.4	11.5	171.4	3	0.58	176.8	2.3	0.17	4.4	0.042	0.038	7.23
4	BG (19)	0.44	0.004	0.075	1.83	57.1	24.8	241.6	0.7	0.02	155.3	1.5	0.59	3.1	0.039	0.042	7.5
	254 days	12.95	0.011	0.169	1.89	37.2	5.5	196.9	1.2	0.44	175.7	1.5	0.18	3.7	0.036	0.057	7.24
6	BG (19)	0.6	0.001	0.177	2.75	97.1	19.7	403.3	6.7	0.01	186.6	1.6	0.63	4.4	0.099	0.180	7.3
	254 days	3.03	0.009	0.19	2.77	79.9	6.3	460.9	3.6	0.65	224.7	2.7	0.08	5.4	0.075	0.173	6.95
8	BG (55)	0.43	0.007	1.177	6.99	321.8	65.2	1098.8	6.9	0.04	336.4	6.4	0.93	5.9	2.84	5.02	7.1
	254 days	15.86	0.091	2.742	9.33	365.1	56.7	1944.2	11.3	2.08	454.6	13.5	0.22	7.7	2.70	5.53	6.81

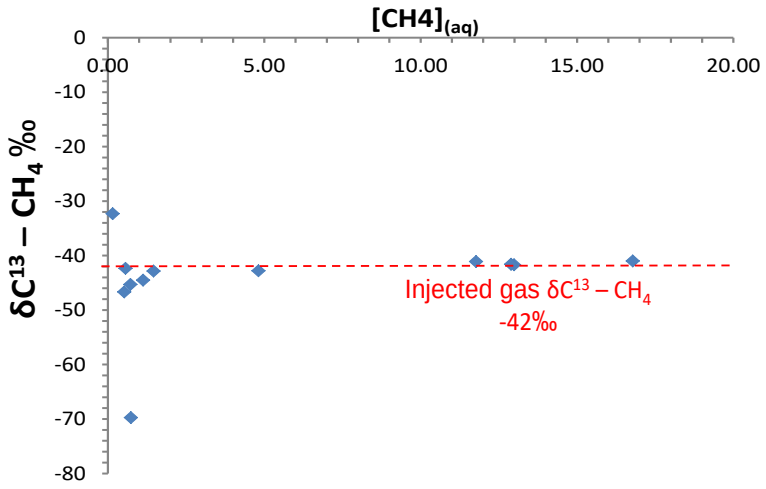

Extended Data Fig. 3: $\delta^{13}C$-CH_4 values (units ‰) on day 245 around the injection area showing that increased methane concentrations in groundwater are associated with $\delta^{13}C$ values of dissolved methane of -42 ‰, identical to the C isotope ratio of the injected CH_4. Except for one

sample, no ^{13}C-enriched carbon isotope ratios of methane were observed, suggesting that methane oxidation in groundwater is very limited.

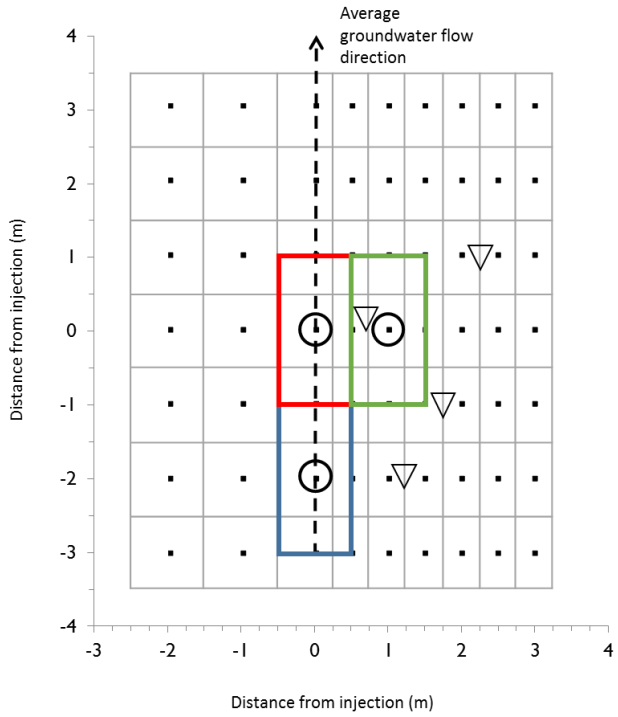

Extended Data Fig. 4: Monitoring network with multilevel soil gas monitoring wells (▽); survey chamber locations (▪) associated with 0.5, 0.75, and 1 m^2 areas for mass balance calculations based on survey efflux measurements (grey rectangles); and LTC locations (○) where red (chamber 1), green (chamber 2), and blue (chamber 3) rectangles indicate the 2 m^2 areas applied for mass balance calculations based on the continuous efflux measurements.

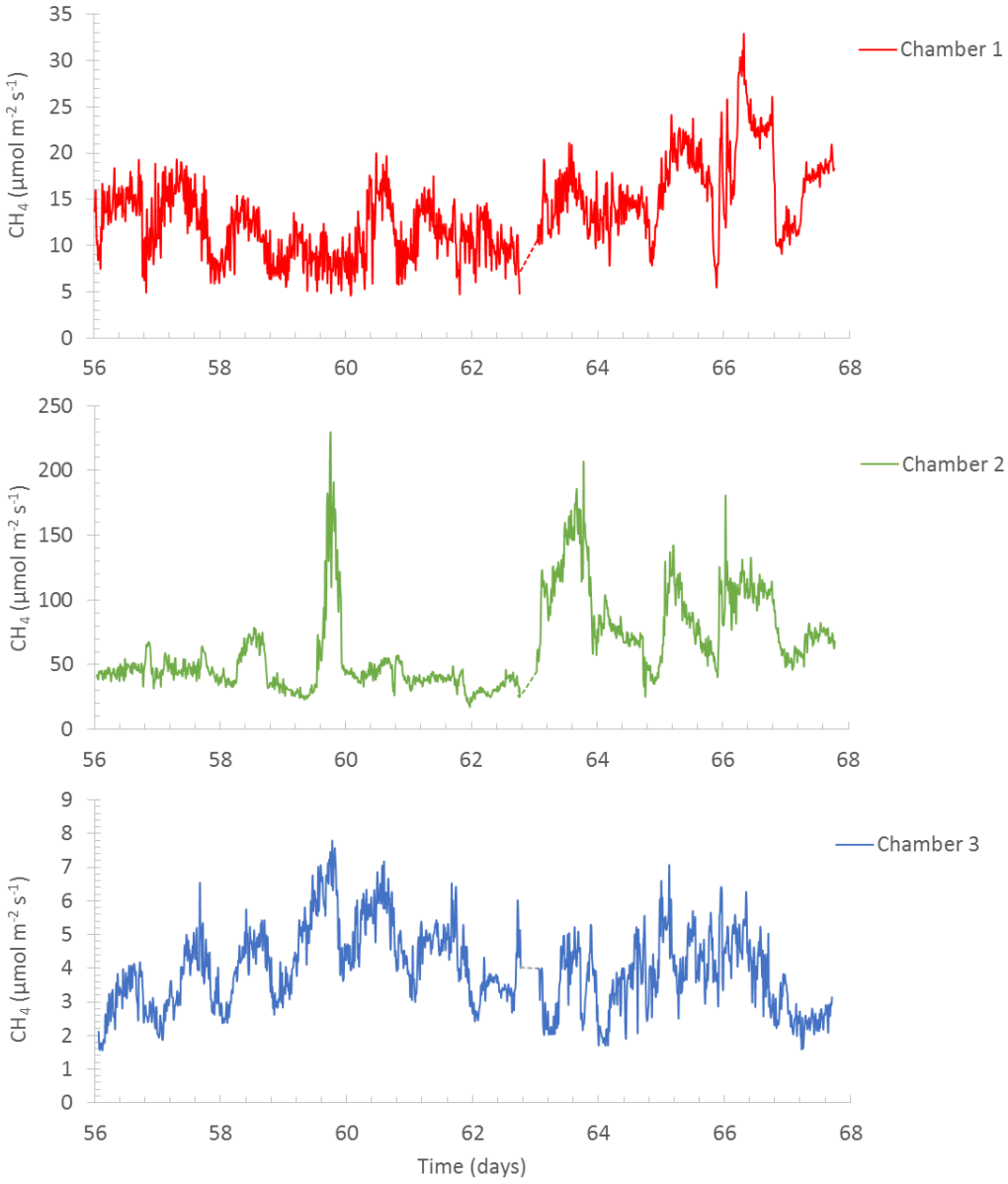

Extended Data Fig. 5: Methane effluxes between day 56 and 68 demonstrate that peak effluxes are not always temporally correlated between the different chamber locations.

Extended Data Table 3: Average rate and cumulative methane loss to the atmosphere from day 56 to 68 (11.75 d) given a 2 m^2 cross sectional area associated with each LTC (Fig. S2), supplemented with survey chamber data. Also shown is the ratio of methane emitted versus methane injected.

	Average Rate $mol \cdot min^{-1}$	Cumulative mol
Emitted at all LTC locations	9.6×10^{-3}	163.0
Emitted at LTC 1	1.6×10^{-3}	27.0
Emitted at LTC 2	7.6×10^{-4}	128.0
Emitted at LTC 3	4.7×10^{-4}	8.0
Emitted at survey chamber locations outside LTC grid	2.0×10^{-4}	3.3
Total emitted (LTC and survey chambers outside LTC grid)	9.8×10^{-3}	166.3
Injected	3.1×10^{-2}	528.4
Ratio methane emitted/injected		**0.31**

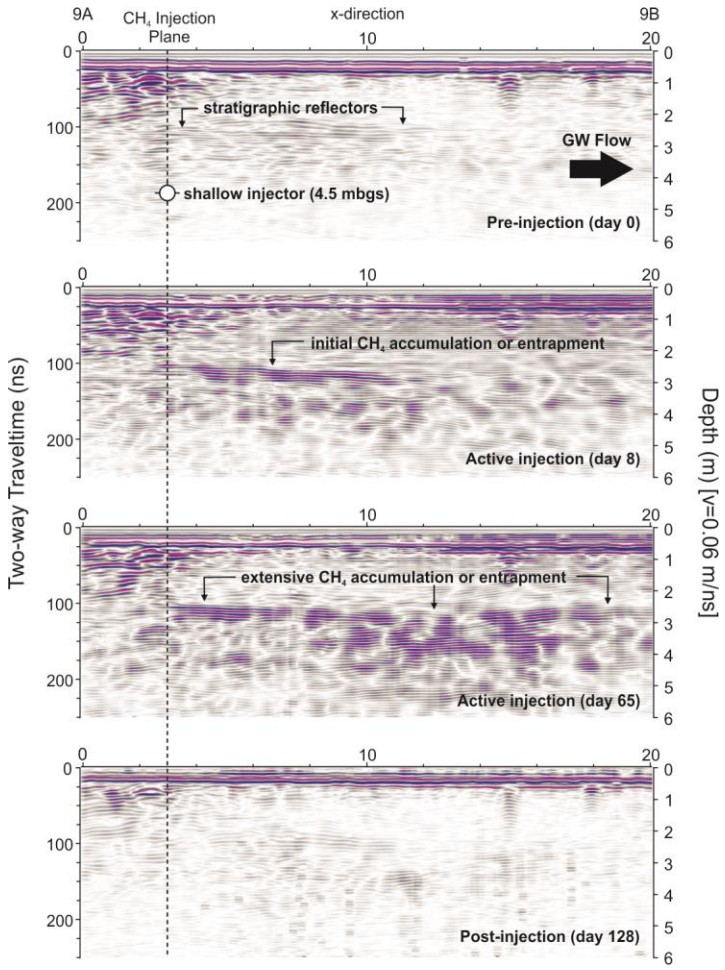

740

741 **Extended Data Fig. 6**: Select GPR reflection profiles parallel to groundwater flow showing
742 changes in reflection amplitude along fixed stratigraphic interfaces. Profile corresponds to the
743 line 1 m west of methane injectors (refer to Fig. 1b). Note transient increase in amplitude along
744 coherent reflection events between 100 and 200 ns during active injection period.

745

746

747

748

Extended Data Table 4: Estimate for the fraction of injected methane lost to the atmosphere on days 56 and 68 from 54 survey chamber locations associated with cross-sectional areas ranging from 0.5 to 1 m^2 (see Fig. S3 for survey grid).

Day	Cumulative efflux $mol \cdot min^{-1}$	Cumulative injection $mol \cdot min^{-1}$	Ratio CH_4 emitted/injected
56	6.8×10^{-3}	3.1×10^{-2}	0.22
68	6.6×10^{-3}	3.1×10^{-2}	0.21

Extended Data Table 5: Cumulative efflux rate and efflux rate outside the LTC area (Fig. S3) based on survey measurements on day 56 and 68. Percentages of cumulative effluxes outside and within the LTC areas are also given.

Day	Cumulative efflux rate $mol \cdot min^{-1}$	Cumulative efflux rate outside LTC area $mol \cdot min^{-1}$	Percentage of cumulative efflux outside LTC area	Percentage of cumulative efflux within LTC area
56	6.8×10^{-3}	2.67×10^{-4}	3.9	96.1
68	6.6×10^{-3}	1.23×10^{-4}	1.9	98.2

Supplementary information

List of all detected operational taxonomic units (OTU at 97% 16S rRNA gene sequence identity) from Borden Aquifer Well M6.